Localization of 5-HT_{1A} Receptors in the Living Human Brain Using [Carbonyl-^{11}C]WAY-100635: PET with Anatomic Standardization Technique

Hiroshi Ito, Christer Halldin and Lars Farde

Karolinska Institutet, Department of Clinical Neuroscience, Psychiatry Section, Karolinska Hospital, Stockholm, Sweden; and Department of Radiology and Nuclear Medicine, Akita Research Institute of Brain and Blood Vessels, Akita City, Japan

Serotonergic 5-hydroxytryptamine-1A (5-HT_{1A}) receptors are of interest in the pathophysiology of several neuropsychiatric disorders such as anxiety, depression and schizophrenia. [Carbonyl-^{11}C]WAY-100635 has recently been shown to be suitable for quantitative determination of 5-HT_{1A} receptors in the human brain using PET. For group comparisons of neuroreceptor distribution on a pixel-by-pixel basis, an anatomic standardization technique is required. In the current study, we have built a database of normal 5-HT_{1A} receptor distribution using [carbonyl-^{11}C]WAY-100635 and an anatomic standardization technique. **Methods:** A PET examination lasting 63 min was performed on six subjects after intravenous injection of [carbonyl-^{11}C]WAY-100635. The radioactivity of the PET images were integrated in the interval 12–63 min and normalized by the radioactivity of the cerebellum, providing a measure of the binding potential (BP) in each pixel. Each PET image was transformed into a standard brain anatomy using a computerized brain atlas system. From the standardized PET images, the sample mean and the SD of the BP were calculated in each pixel. **Results:** On the anatomically standardized average image, high BP was observed in the cerebral cortices, hippocampus and raphe nucleus, whereas low BP was observed in the basal ganglia and thalamus. This regional distribution is in good agreement with the distribution of 5-HT_{1A} receptors known from in vitro studies. **Conclusion:** The anatomic standardization technique permits building of a database of the normal 5-HT_{1A} receptor distribution in the living human brain. This technique can be applied for group comparisons of neuroreceptor distribution on a pixel-by-pixel basis.

Key Words: serotonin 5-HT_{1A} receptor; brain; WAY-100635; PET; anatomic standardization

J Nucl Med 1999; 40:102–109

Serotonergic 5-hydroxytryptamine-1A (5-HT_{1A}) receptors are of interest in the pathophysiology of several neuropsychiatric disorders, such as anxiety, depression and schizophrenia (*1*). WAY-100635 (*N*-(2-(4-(2-methoxyphenyl)-1-piperazinyl)ethyl)-*N*-(2-pyridyl) cyclohexanecarboxamide) is a potent 5-HT_{1A} receptor antagonist (*2*). In vitro, WAY-100635 binds with subnanomolar affinity to 5-HT_{1A} receptors (dissociation constant [K_d] = 0.4 nmol/L) (*3*), whereas its affinity for other putative receptors is at least 100-fold lower. The labeling of WAY-100635 in the carbonyl position with ^{11}C that avoids formation of lipophilic radioactive metabolites provides a radioligand, [carbonyl-^{11}C]WAY-100635, which is suitable for quantitative determination of 5-HT_{1A} receptors in the human brain (*4–8*).

Fox et al. (*9*) have reported that intersubject averaging of PET images, a technique requiring transformation of brain images of individual subjects into a standard brain shape and size in three dimensions (anatomic standardization), gives enhanced detection of focal brain responses. This anatomic standardization technique permits group comparisons between normal control subjects and patients on a pixel-by-pixel basis (*10–12*). Recently, assessment of neuroreceptor distribution using PET and the anatomic standardization technique has also been proposed (*13*).

The Computerized Brain Atlas (CBA) system for anatomic standardization has been developed at our center (*14,15*) and used for brain activation studies with PET (*16*). This system is based on digitized sections from a cryosected postmortem brain and can be used to transform anatomic brain structures of subjects into a standard anatomic format using linear and nonlinear parameters. In this study, we used this CBA system to build a database of normal 5-HT_{1A} receptor distribution in the living human brain using [carbonyl-^{11}C]WAY-100635. The study is based on a previously published kinetic analysis of [carbonyl-^{11}C]WAY-100635 (*7,8*).

MATERIALS AND METHODS

Subjects

The study was approved by the Ethics and Radiation Safety Committees of the Karolinska Hospital. Six healthy men (20–42 y) were recruited and gave written informed consent. The subjects were healthy according to medical history, physical examination, blood and urine screening analyses and MRI of the brain. They did not use any medication.

Radiochemistry

[Carbonyl-^{11}C]WAY-100635 was prepared by ^{11}C-acylation of the descyclohexanecarbonyl analogue of WAY-100635 (WAY-

Received Nov. 3, 1997; revision accepted Apr. 28, 1998.

For correspondence or reprints contact: Hiroshi Ito, MD, Department of Radiology and Nuclear Medicine, Akita Research Institute of Brain and Blood Vessels, 6-10 Senshu-kubota-machi, Akita City, Akita 010, Japan.

100634) with [carbonyl-^{11}C]cyclohexanecarbonyl chloride as described in detail elsewhere (*6*). The specific radioactivity of [carbonyl-^{11}C]WAY-100635 was 26–100 GBq/μmol at the time of injection.

PET Procedure

After intravenous bolus injection of 219–307 MBq [carbonyl-^{11}C]WAY-100635, the brain radioactivity was measured for 63 min in a consecutive series of time frames. The frame sequence consisted of three 1-min frames, four 3-min frames, and eight 6-min frames. The PET system used was an ECAT Exact HR (Siemens Medical Systems, Inc., Iselin, NJ), which provides 47 slices with a center-to-center distance of 3.125 mm (*17*). The intrinsic spatial resolution was 3.6 mm in plain and 4.0 mm full width at half maximum (FWHM) axially. With a Hanning filter, the reconstruction in plain resolution was 5.5 mm FWHM. The image matrix size was 128 × 128, and the pixel size was 2.0 mm. Data were acquired in three-dimensional mode. Scatter correction was done (*18*). Attenuation correction was performed using the transmission scan data that were obtained for each subject. A head-fixation system with an individual plaster helmet was used in the PET and MRI examinations to allow the mastering of positioning between the two modalities (*19*).

To obtain the arterial input function, an automated blood sampling system was used during the first 5 min of each measurement (*20*). Thereafter, arterial blood samples were taken manually at the midpoint of each frame until the end of the measurement (*21*). The fraction of radioactivity representing unchanged [carbonyl-^{11}C]WAY-100635 in plasma was determined by gradient high-performance liquid chromatography as described previously (*4,22*).

MRI Examination

T2-weighted images of the brain were obtained for all subjects. The MRI system used was Signa, 1.5 T (GE Medical Systems, Milwaukee, WI). The pulse sequence used was the fast spin-echo method (repetition time = 3000 ms, echo time = 90 ms). The positioning of the head and the series of sections was the same as in the PET studies. The slice interval and thickness were 3.1 mm and 3.0 mm, respectively. The field of view was 26 cm, and the image matrix size was 256 × 256.

Calculation of Parametric PET Image

The time-activity curves of several neuroreceptor ligands have been described by using the standard three-compartment model with four first-order rate constants (K_1, k_2, k_3 and k_4) (*21,23–25*). The rate constants K_1 and k_2 correspond to the influx and efflux rate for radioligand diffusion through the blood-brain barrier. The rate constants k_3 and k_4 correspond to the rate for radioligand transfer between the compartments for nondisplaceable radioligand and specific radioligand binding to receptors. On the basis of this model, the binding potential (BP) in a brain region is expressed as follows:

$$BP = k_3/k_4. \quad \text{Eq. 1}$$

The quantification of neuroreceptors using a reference region is a conventional approach for applied clinical neuroimaging. Because the density of 5-HT$_{1A}$ receptor in the cerebellum is very low (*5,6,26–29*), the cerebellum (cerebellar cortex) was used as a reference region for calculation of BP. The BP can be expressed as follows (*30*):

$$BP = V_{d(region)}/V_{d(cerebellum)} - 1, \quad \text{Eq. 2}$$

where $V_{d(region)}$ and $V_{d(cerebellum)}$ are the total distribution volumes for a brain region and for the cerebellum, respectively. The total distribution volume V_d is calculated from four rate constants as follows:

$$V_d = (K_1/k_2)/(1 + k_3/k_4). \quad \text{Eq. 3}$$

The rate constants K_1, k_2, k_3 and k_4 can be calculated by a conventional nonlinear least squares fitting procedure.

Because calculation of V_d values on a pixel-by-pixel basis by a nonlinear least squares fitting procedure is time consuming, a simplified approach to calculate the BP was applied. The BP in a brain region was calculated by the integration of the time-activity curves in each pixel as follows (*21,30*):

$$BP = \int C_{t(region)}(t)dt \Big/ \int C_{t(cerebellum)}(t)dt - 1, \quad \text{Eq. 4}$$

where $C_{t(region)}$ and $C_{t(cerebellum)}$ are the radioactivity concentrations for a brain region and for the cerebellum, respectively. To calculate the images of BP, the time-activity data for each pixel were integrated before anatomic standardization and then divided by the integrated radioactivity for the cerebellum; 1 was subtracted after anatomic standardization. The optimal integration interval was determined both from the analysis of experimental data and from the simulation study, as described in the following.

Experimental Data Analysis. To determine the optimal integration interval, the BP values calculated from the integration of the time-activity curves (Eq. 4) were compared with those calculated from the total distribution volumes (Eq. 2).

The integration intervals used were 9–63, 12–63, 21–63 and 33–63 min in equation 4, although equation 4 is theoretically correct only for the integration interval from 0 to infinity. Because the image obtained by the integration for the late part of the time-activity data was similar to the image of distribution volume (*31*), the end time of integration interval was fixed at 63 min. Because the image obtained by the integration for the early part of the time-activity data can be affected by the change of cerebral blood flow (*31*), the data of 0–9 min were not used.

The total distribution volume values were calculated from four rate constants obtained by a conventional nonlinear least squares fitting procedure for measured uptake curves (Eq. 3) (*32*). The radioactivity of unchanged [carbonyl-^{11}C]WAY-100635 in plasma was used as the arterial input function (*8,21*). To diminish the influence of tracer remaining in the blood, the first frame (0–60 s) of the regional time-activity curves was excluded (*8,33*).

Simulation Study. To determine the optimal integration interval, the errors of the BP calculated by equation 4 using the integration intervals (9–63, 12–63, 21–63 and 33–63 min) were estimated by a simulation study. Tissue time-activity curves for brain regions (0–60 min) were generated according to the three-compartment model. The K_1/k_2 and k_4 values were assumed to be 0.444 mL/mL and 0.023 min^{-1}, respectively. The tissue time-activity curves were generated with K_1 values between 0.10 and 0.22 mL/mL/min in seven steps and with k_3 values between 0.06 and 0.30 min^{-1} in five steps. A tissue time-activity curve for the cerebellum was also generated according to the three-compartment model using 0.16 mL/mL/min, 0.36 min^{-1}, 0.046 min^{-1} and 0.046 min^{-1} as values of K_1, k_2, k_3 and k_4, respectively. These assumed values were taken from the conventional nonlinear least squares fitting analysis of measured uptake curves for all regions of interest. A typical input function was used for generating tissue time-activity curves. The

BP were then calculated by equation 4 for each integration interval, using these generated tissue time-activity curves. These estimated BP values were compared with the BP values calculated by equation 2.

Effect of Intravascular Radioactivity

Because the radioactivity concentration in the cerebellum was lower than that of unchanged ligand and metabolites remaining in the blood at a late phase after injection of [carbonyl-^{11}C]WAY-100635 (*8*), the effect of intravascular radioactivity in the cerebellum cannot be ignored in even late phase. To estimate the effect of intravascular radioactivity for calculation of BP using equation 4, a simulation study was performed. The intravascular radioactivity was calculated using standard values for regional cerebral blood volume (CBV) (*34,35*) and a typical curve for measured radioactivity in arterial whole blood. The thereby calculated radioactivity in the blood was thereafter subtracted from the regional time-activity curves, which were generated according to the three-compartment model as described earlier. The BP values were then calculated by equation 4.

Anatomic Standardization

PET images obtained by integration of the time-activity data for each pixel were transformed into the standard brain size and shape using the CBA system (*14,15*). The anatomic structures of the computerized standard brain atlas, i.e., contour of the brain, main sulci, ventricles, basal ganglia and thalamus, were fitted interactively to each subject's MR image using both linear and nonlinear transformation in three-dimensional space. The transformation parameters were subsequently used to transform each subject's PET image into the standard atlas form. Because the positioning of the head and the series of sections was the same between PET and MRI using a head-fixation system (*19*), alignment of image slices between PET and MRI was done only when necessary using the contour of the whole brain before transformation of the PET image. For confirmation of correct transformation into the standard brain atlas form, each subject's MR image was also transformed using the same parameters.

After the anatomic standardization procedure, all subjects' PET images had the same anatomic brain format. To calculate images of BP, the radioactivity in each pixel was divided by the radioactivity in the cerebellum and subtracted by 1. Then, the average and the SD images of the sample were calculated on a pixel-by-pixel basis.

Regions of Interest

Regions of Interest on the Original PET Images. Regions of interest (ROIs) were drawn on the MR images and transferred to the original PET images. ROIs were defined for the frontal cortex, lateral temporal cortex, medial temporal cortex including hippocampus and cerebellar cortex. Because the positioning of the head and the series of sections was the same between PET and MRI using a head-fixation system (*19*), alignment for position of ROIs between PET and MRI was done only when necessary using the contour of whole brain. ROI for the raphe nucleus was directly drawn on the original PET images. Each ROI was drawn in three adjacent sections and the data were pooled, so that the mean radioactivity concentration for the whole volume of interest was obtained. To obtain regional time-activity curves, regional radioactivity was calculated for each frame, corrected for decay and plotted versus time.

Regions of Interest on the Anatomically Standardized PET Images. To compare the regional radioactivity on the original PET images and on the anatomically standardized PET images, ROIs were drawn on the standard brain atlas using the same criteria as on the original PET images. These ROIs were transferred to the anatomically standardized PET images for each subject. ROI for the raphe nucleus was drawn directly on the anatomically standardized PET images. Each ROI was drawn in three adjacent sections with each interval of 3.0 mm, and the data were pooled, so that the mean radioactivity concentration for the whole volume of interest was obtained.

Detailed Regions of Interest on the Anatomically Standardized Average PET Image. To compare the anatomically standardized average PET image with the previously reported in vitro distribution of 5-HT_{1A} receptor in humans, ROIs were drawn for detailed structures on the standard brain atlas and transferred to the average and the SD images. ROIs were defined for the cerebral cortices of main gyri, cerebral white matter, insula, hippocampus, amygdaloid nucleus, basal ganglia and thalamus. ROI for the raphe nucleus was drawn directly on the average image and transferred to the SD images. Each ROI was drawn in three adjacent sections with each interval of 3.0 mm and the data were pooled, so that the mean value for the whole volume of interest was obtained.

RESULTS

Time curves for regional brain radioactivity for one subject are shown in Figure 1. The rate constants, the total distribution volume (*8*) and the BP calculated from the total distribution volumes (Eq. 2) are given in Table 1.

The comparisons between BP values obtained by the integration of the time-activity curves (Eq. 4) for each integration interval and by the total distribution volumes (Eq. 2) are shown in Figure 2. BP calculated from the integrated data in the time interval 12–63 min were in good agreement with those calculated from the total distribution volumes. Coefficients of variation of BP in the six subjects for each integration interval are shown in Figure 3. Using the integrated data in the 12- to 63-min interval, the coefficient of variation was found to be approximately 20%.

Errors of BP calculated by the integration of the time-activity curves (Eq. 4) for each integration interval were simulated (Fig. 4). With the integration interval 12–63 min, the estimated BP values were in good agreement with the BP

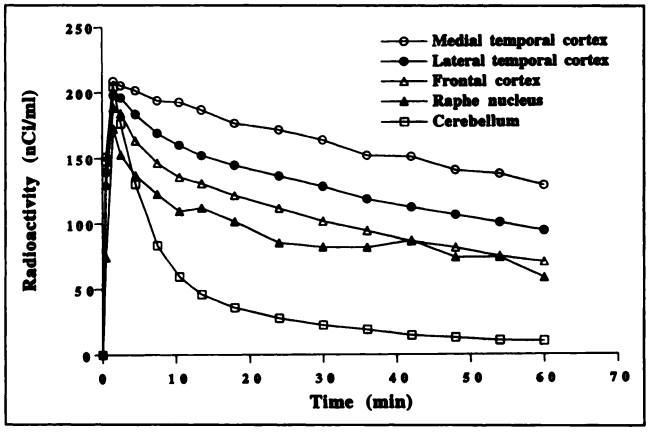

FIGURE 1. Time curves for regional brain radioactivity after intravenous injection of 305 MBq [carbonyl-^{11}C]WAY-100635 for one subject.

TABLE 1
Rate Constants, Total Distribution Volume (V_d) and Binding Potential (BP) Calculated from V_d

Region	K_1 (mL/mL/min)	k_2 (min^{-1})	k_3 (min^{-1})	k_4 (min^{-1})	V_d (mL/mL)	BP
Frontal cortex	0.16 ± 0.04	0.36 ± 0.05	0.19 ± 0.03	0.02 ± 0.002	3.93 ± 1.21	3.12 ± 0.60
Lateral temporal cortex	0.15 ± 0.03	0.31 ± 0.06	0.22 ± 0.03	0.02 ± 0.004	5.77 ± 2.29	4.99 ± 1.39
Medial temporal cortex	0.14 ± 0.04	0.30 ± 0.10	0.27 ± 0.06	0.02 ± 0.003	7.55 ± 2.11	6.94 ± 1.11
Raphe nucleus	0.14 ± 0.06	0.41 ± 0.24	0.16 ± 0.07	0.02 ± 0.004	4.20 ± 1.59	3.36 ± 1.00
Cerebellum	0.17 ± 0.04	0.39 ± 0.05	0.05 ± 0.02	0.05 ± 0.005	0.88 ± 0.20	—

Values are mean ± SD.
BP = $V_{d(region)}/V_{d(cerebellum)}^{-1}$.

calculated from the total distribution volumes. Errors of BP calculated by the integrated data in the 12- to 63-min interval, when the assumed BP and K_1 in a brain region were varied, were simulated (Fig. 5). The errors of the estimated BP for different BP and K_1 were found to be approximately ±10%, excluding low K_1 and high BP. The largest underestimation was observed for low K_1 and high BP.

Errors of BP calculated by the integration of the time-activity curves in the 12- to 63-min interval at CBV values ranging from 0% to 7% were simulated (Fig. 6). When no correction was made for the intravascular radioactivity (CBV = 0%), the BP was underestimated by 17% compared with an estimate with a correction of intravascular radioactivity using an assumed CBV value of 5%. The error was only ±4% when CBV was changed from 4% to 6%.

The correlation between the radioactivity in each ROI both on the original PET images and on the anatomically standardized PET images are shown in Figure 7. PET images were obtained by integration of the time-activity data for 12–63 min. The radioactivity levels on both images were in good agreement.

The average image of the parametric PET images, which were anatomically standardized, is shown in Figure 8. For calculation of the parametric PET images, the integration interval of 12–63 min was used. Table 2 gives the values for each ROI, which were drawn for detailed structures on the average (Fig. 8) and SD images. High BP was observed in the cerebral cortices, hippocampus and raphe nucleus, whereas low BP was observed in the basal ganglia and thalamus.

DISCUSSION

Tracer Kinetics

The specific binding (the ratio of k_3/k_4) of [carbonyl-^{11}C]WAY-100635 in the cerebellum was 7 to 14 times lower than that in the cerebral cortices (Table 1) (*7,8*). This indicates that the density of 5-HT_{1A} receptors in the cerebellum is very low (*6,26,36*), and therefore, the cerebellum was used as a reference region.

The radioactivity in the cerebral cortices was 8 to 13 times higher than that in the cerebellum at the end of measurement (n = 6) (Fig. 1), and the total distribution volume for the cerebral cortices was 4 to 9 times higher than that for the cerebellum (Table 1). The BP calculated from the total distribution volumes for the cerebral cortices was high (3

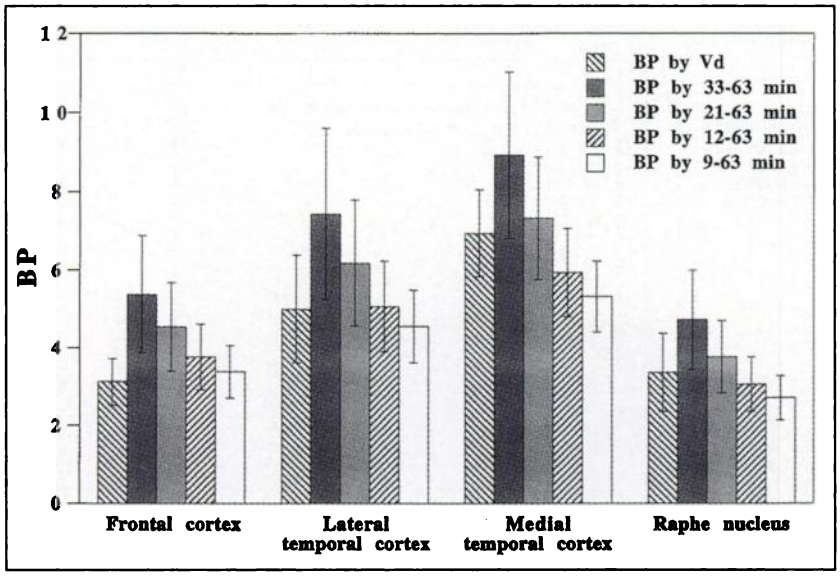

FIGURE 2. Comparison between BP values obtained by integration of time-activity curves for each integration interval and by total distribution volumes (mean ± SD).

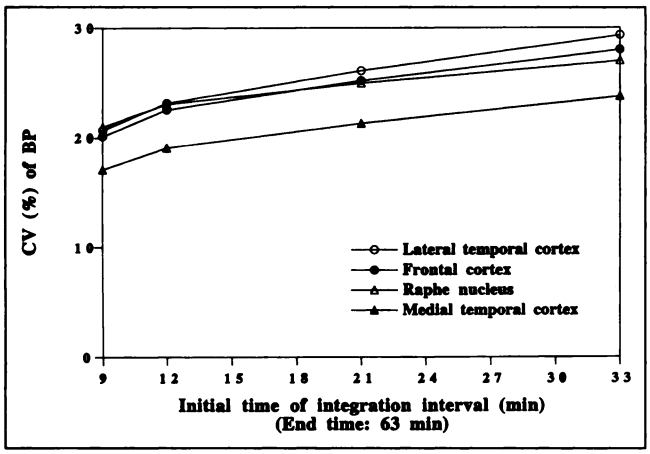

FIGURE 3. Coefficients of variation (CV [%]) of BP in six subjects for each integration interval.

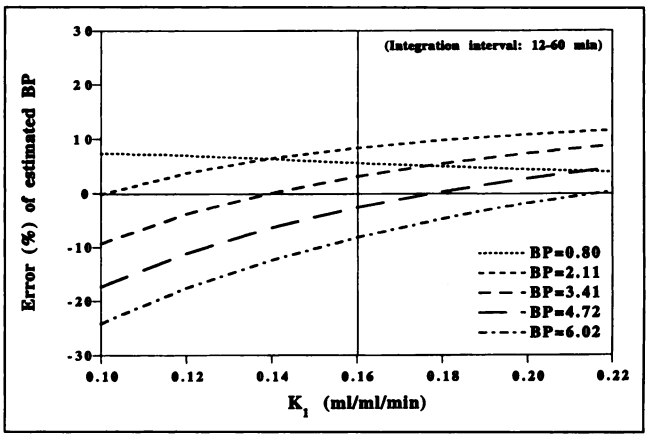

FIGURE 5. Errors of BP calculated by integration of time-activity curves in time interval 12–63 min for different BP and K_1.

to 7) (Table 1). These values indicate that [carbonyl-^{11}C]WAY-100635 is suitable for quantitative determination of 5-HT_{1A} receptors (*8*).

Calculation of Parametric PET Image

In both the experimental data analysis and the simulation study (Figs. 2 and 4), the BP values calculated by the integration of the time-activity curves in the 12- to 63-min interval were in good agreement with those calculated by the total distribution volumes. Although the integration intervals of late phase are often used for estimation of binding characteristic with PET, the overestimation of BP was observed when the integration intervals of late phase (21–63 and 33–63 min) were used (Figs. 2 and 4) (*37*). In addition, the integration interval of 12–63 min provided a lower coefficient of variation of BP in the six subjects compared with the integration intervals of late phase (Fig. 3). Although the integration interval of 9–63 min actually provided the best coefficient of variation of BP (Fig. 3), this interval caused an underestimation of BP (Figs. 2 and 4). We concluded that the optimal integration interval for [carbonyl-^{11}C]WAY-100635 is 12–63 min.

Drug-induced 5-HT_{1A} receptor occupancy is calculated by $1 - BP_{(drug)}/BP_{(control)}$ (*38*). Assumed BP values of 0.80, 2.11, 3.41 and 4.72 give estimated BP values of 0.85, 2.28, 3.52 and 4.59, respectively, which were calculated by equation 4 using the integration interval of 12–63 min (Fig. 4). When an assumed BP value of 4.72 is regarded as the control value, assumed BP values of 0.80, 2.11 and 3.41 correspond to receptor occupancy values of 83%, 55% and 28%, respectively. Conversely, when a estimated BP value of 4.59 is regarded as the control value, estimated BP values of 0.85, 2.28 and 3.52 correspond to receptor occupancy values of 81%, 50% and 23%, respectively. Although the receptor occupancy calculated by using the integration interval of 12–63 min is slightly underestimated, this integration interval can be used for the determination of drug-induced 5-HT_{1A} receptor occupancy.

The errors of BP calculated by the integration of the time-activity curves in the 12- to 63-min interval for different BP and K_1 were approximately ±10%, excluding low K_1 and high BP (Fig. 5). This indicates that the use of the integration interval 12–63 min can provide accurate BP, even if the K_1 and BP values in a brain region are changed because of neurological and psychiatric diseases. However,

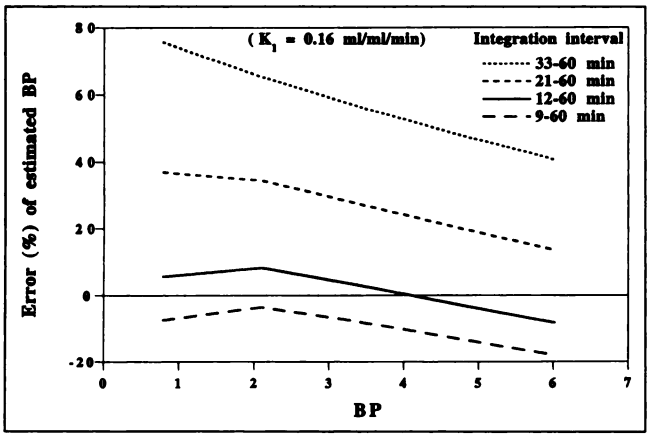

FIGURE 4. Errors of BP calculated by integration of time-activity curves for each integration interval.

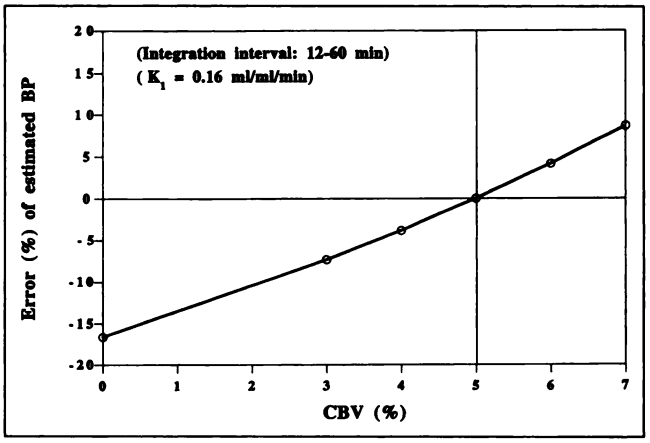

FIGURE 6. Errors of BP calculated by integration of time-activity curves in interval 12–63 min at CBV values ranging from 0% to 7%. Errors are expressed for CBV of 5%.

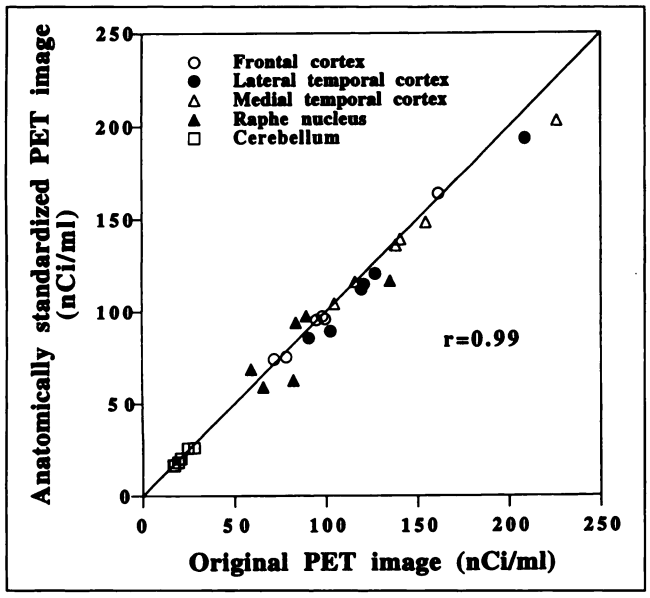

FIGURE 7. Correlation between radioactivity for each ROI both on original PET images and on anatomically standardized PET images. Values are mean radioactivity (nCi/mL) for interval 12–63 min. Solid line is identity.

when the BP is high at the same time the K_1 is low, use of the integration interval 12–63 min will cause significant underestimation of BP. This might be a problem in PET research on schizophrenia and depression, because hypoperfusion in the prefrontal cortex has been reported for these diseases (*12,39*).

Effect of Intravascular Radioactivity

To correct for the effect of radioactivity in CBV, two approaches were applied in this study (*8*). The first was to exclude the first frame of the regional time-activity curves (*33*). The second was to use standard values for regional CBV (*34,35*) and the curve for measured radioactivity in arterial whole blood. The thereby calculated radioactivity in the blood was thereafter subtracted from the regional time-activity curves. Both approaches gave almost identical results in the kinetic analysis according to the three-compartment model (*8*). However, the total V_d for the cerebellum was slightly different between the two approaches because of the intravascular radioactivity, whereas the K_1 and BP ($=k_3/k_4$) were almost identical between the two approaches (data not shown). A particular problem with [carbonyl-^{11}C]WAY-100635 is that the radioactivity concentration in the cerebellum was lower than that of unchanged ligand and metabolites remaining in the blood at a late phase after injection (*8*). An effect of intravascular radioactivity in the cerebellum thus cannot be ignored in even late phase.

If no correction is applied for intravascular radioactivity, the BP will be underestimated (Fig. 6). However, normal value of CBV has been reported to be approximately 5% ± 1% (*34,35*), and the error will only be ±4% when CBV is changed between 4% and 6% (Fig. 6). This indicates that there is systematic underestimation of BP calculated by equation 4 attributable to the intravascular radioactivity in the cerebellum, but a change of CBV will not significantly affect the BP.

Anatomic Standardization

The CBA system transforms the brain anatomic structures of subjects into a standard anatomic format, and this procedure might change regional brain radioactivity. In the current study, the regional radioactivity both on the original PET images and on the anatomically standardized PET images were in good agreement (Fig. 7), indicating that the anatomic standardization technique does not change the regional brain radioactivity appreciably (*14*).

Localization of 5-HT$_{1A}$ Receptors

The distribution of 5-HT$_{1A}$ receptors has been investigated in rat, monkey and human in vitro using [^{3}H]8-OH-DPAT and [*O*-methyl-^{3}H]WAY-100635 (*6,26,27,36,40,41*). High densities have been found in the cerebral cortices, hippocampus and raphe nucleus.

WAY-100635 has high affinity and selectivity for the 5-HT$_{1A}$ receptor in vitro (*2*). ^{11}C-labeled WAY-100635, [carbonyl-^{11}C]WAY-100635, is suitable for quantitative determination of 5-HT$_{1A}$ receptors in the living human brain (*4–8*). In this study, high BP was observed in the cerebral cortices, hippocampus and raphe nucleus, whereas low BP was observed in the basal ganglia and thalamus (Fig. 8, Table 2). This regional distribution is in good agreement with the known distribution of 5-HT$_{1A}$ receptors and supports that the ligand binds selectively to 5-HT$_{1A}$ receptors in the human brain.

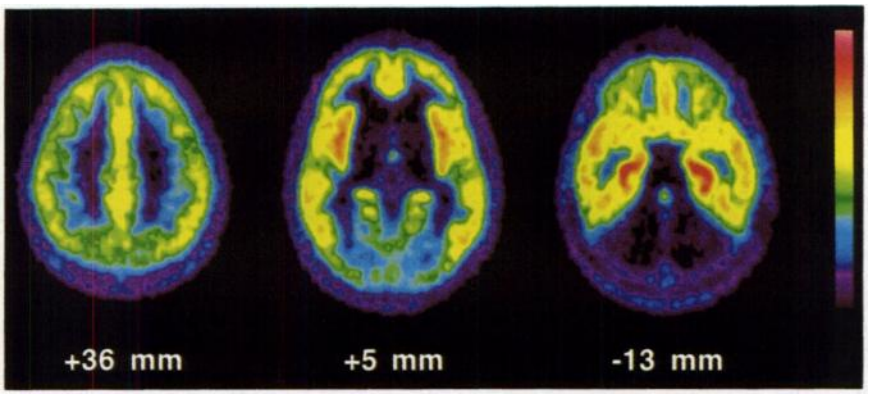

FIGURE 8. Average image of parametric PET images (BP images) that were anatomically standardized. Image slices are transverse +36, +5 and −13 mm relative to anteroposterior commissure line. Subjects' right is on the left. Scale maximum and minimum values are 8.32 and 0, respectively.

TABLE 2
Values for Each Region of Interest Drawn for Detailed Structures on the Average and SD Images of Binding Potential

Region	Average	SD
Frontal cortex		
Superior frontal gyrus	4.06	1.37
Middle frontal gyrus	4.03	1.48
Inferior frontal gyrus	4.21	1.36
Cingulate gyrus	4.32	1.28
Rectal gyrus	4.83	1.35
Orbital gyrus	4.04	1.06
Precentral gyrus	3.66	1.07
Temporal cortex		
Superior temporal gyrus	5.49	1.70
Middle temporal gyrus	5.09	1.68
Inferior temporal gyrus	4.49	1.55
Parahippocampal gyrus	5.40	1.64
Parietal cortex		
Angular gyrus	4.25	1.24
Supramarginal gyrus	4.16	1.39
Postcentral gyrus	3.97	1.35
Occipital cortex		
Lingual gyrus	2.82	0.91
Cuneus	3.09	0.97
Centrum semiovale	0.35	0.83
Insular cortex	6.01	1.65
Hippocampus	6.43	1.60
Amygdaloid nucleus	5.77	1.33
Putamen	0.60	0.72
Caudate nucleus	0.30	0.62
Globus pallidus	0.23	0.70
Thalamus	0.61	0.73
Raphe nucleus	3.01	1.36

Values are mean for all pixel values in a region of interest on each image.

The cerebellum was used as a reference region. The density of 5-HT_{1A} receptors of the cerebellum has been reported to be very low but not zero (*6,26,36*). In addition, the ratio of k_3/k_4 in the cerebellum was very low but not zero (Table 1) (*8*). This might cause errors in calculating BP. The assumption of negligible radioligand binding in the cerebellum has been discussed in the literature (*8*).

The anatomic standardization technique permits construction of a database of the normal 5-HT_{1A} receptor distribution in the living human brain. This technique can be applied for group comparisons of neuroreceptor distribution between normal control subjects and patients on a pixel-by-pixel basis.

CONCLUSION

We have built a database of normal 5-HT_{1A} receptor distribution using [carbonyl-^{11}C]WAY-100635 and an anatomic standardization technique. On the anatomically standardized average image, high BP was observed in the cerebral cortices, hippocampus and raphe nucleus, whereas low BP was observed in the basal ganglia and thalamus. This regional distribution is in good agreement with the known distribution of 5-HT_{1A} receptors. With the anatomic standardization technique, a database of the normal 5-HT_{1A} receptor distribution was constructed. This technique can be applied for group comparisons of neuroreceptor distribution between normal control subjects and patients on a pixel-by-pixel basis.

ACKNOWLEDGMENTS

This work was supported by grants from the Swedish Medical Research Council (09114-0613), the Swedish Natural Science Research Council (K-KU 9973-308), the United States National Institute of Mental Health (NIMH 41205-11) and Karolinska Institutet. The assistance of the members of the Karolinska PET group involved in the PET experiments is also gratefully acknowledged.

REFERENCES

1. Saxena PR. Serotonin receptors: subtypes, functional responses and therapeutic relevance. *Pharmacol Ther.* 1995;66:339–368.
2. Forster EA, Cliffe IA, Bill DJ, et al. A pharmacological profile of the selective silent 5-HT_{1A} receptor antagonist, WAY-100635. *Eur J Pharmacol.* 1995;281: 81–88.
3. Khawaja X, Evans N, Reilly Y, Ennis C, Minchin MC. Characterisation of the binding of [^{3}H]WAY-100635, a novel 5-hydroxytryptamine$_{1A}$ receptor antagonist, to rat brain. *J Neurochem.* 1995;64:2716–2726.
4. Osman S, Lundkvist C, Pike VW, et al. Characterization of the radioactive metabolites of the 5-HT_{1A} receptor radioligand, [*O*-methyl-^{11}C]WAY-100635, in monkey and human plasma by HPLC. Comparison of the behavior of an identified radioactive metabolite with parent radioligand in monkey using PET. *Nucl Med Biol.* 1996;23:627–634.
5. Pike VW, McCarron JA, Lammertsma AA, et al. Exquisite delineation of 5-HT_{1A} receptors in human brain with PET and [carbonyl-C-11]WAY-100635. *Eur J Pharmacol.* 1996;301:R5–R7.
6. Hall H, Lundkvist C, Halldin C, et al. Autoradiographic localization of 5-HT_{1A} receptors in the post-mortem human brain using [^{3}H]WAY-100635 and [^{11}C]WAY-100635. *Brain Res.* 1997;745:96–108.
7. Ito H, Halldin C, Lundkvist C, Swahn CG, Pike V, Farde L. 5-HT_{1A} receptor imaging in the human brain using [C-11]WAY-100635 and PET [Abstract]. *J Nucl Med.* 1997;38:286P.
8. Farde L, Ito H, Swahn CG, Pike VW, Halldin C. Quantitative analyses of carbonyl-carbon-11-WAY-100635 binding to central 5-hydroxytryptamine-1A receptors in man. *J Nucl Med.* 1998;39:1965–1971.
9. Fox PT, Mintun MA, Reiman EM, Raichle ME. Enhanced detection of focal brain responses using intersubject averaging and change-distribution analysis of subtracted PET images. *J Cereb Blood Flow Metab.* 1988;8:642–653.
10. Bench CJ, Friston KJ, Brown RG, Scott LC, Frackowiak RS, Dolan RJ. The anatomy of melancholia: focal abnormalities of cerebral blood flow in major depression. *Psychol Med.* 1992;22:607–615.
11. Dolan RJ, Bench CJ, Brown RG, Scott LC, Friston KJ, Frackowiak RS. Regional cerebral blood flow abnormalities in depressed patients with cognitive impairment. *J Neurol Neurosurg Psychiatry.* 1992;55:768–773.
12. Ito H, Kawashima R, Awata S, et al. Hypoperfusion in the limbic system and prefrontal cortex in depression: SPECT with anatomic standardization technique. *J Nucl Med.* 1996;37:410–414.
13. Frey KA, Minoshima S, Koeppe RA, Kilbourn MR, Berger KL, Kuhl DE. Stereotaxic summation analysis of human cerebral benzodiazepine binding maps. *J Cereb Blood Flow Metab.* 1996;16:409–417.
14. Seitz RJ, Bohm C, Greitz T, et al. Accuracy and precision of the computerized brain atlas programme for localization and quantification in positron emission tomography. *J Cereb Blood Flow Metab.* 1990;10:443–457.
15. Greitz T, Bohm C, Holte S, Eriksson L. A computerized brain atlas: construction, anatomical content, and some applications. *J Comput Assist Tomogr.* 1991;15: 26–38.
16. Ingvar M, Eriksson L, Greitz T, et al. Methodological aspects of brain activation studies: cerebral blood flow determined with [^{15}O]butanol and positron emission tomography. *J Cereb Blood Flow Metab.* 1994;14:628–638.
17. Wienhard K, Dahlbom M, Eriksson L, et al. The ECAT EXACT HR: performance of a new high resolution positron scanner. *J Comput Assist Tomogr.* 1994;18:110–118.
18. Watson CC, Newport D, Casey ME. A single scatter simulation technique for scatter correction in 3D PET. In: Grangeat P, Amans JL, eds. *Three-Dimensional*

Image Reconstruction in Radiology and Nuclear Medicine. Dordrecht, The Netherlands: Kluwer Academic Publishers; 1996:255–268.
19. Bergstrom M, Boethius J, Eriksson L, Greitz T, Ribbe T, Widen L. Head fixation device for reproducible position alignment in transmission CT and positron emission tomography. *J Comput Assist Tomogr.* 1981;5:136–141.
20. Eriksson L, Holte S, Bohm C, Kesselberg M, Hovander B. Automatic blood sampling systems for positron emission tomography. *IEEE Trans Nucl Sci.* 1988;35:703–707.
21. Farde L, Eriksson L, Blomquist G, Halldin C. Kinetic analysis of central [^{11}C]raclopride binding to D_2-dopamine receptors studied by PET—a comparison to the equilibrium analysis. *J Cereb Blood Flow Metab.* 1989;9:696–708.
22. Halldin C, Swahn CG, Farde L, Sedvall G. Radioligand disposition and metabolism: key information in early drug development. In: Comer D, ed. *PET for Drug Development and Evaluation.* Dordrecht, The Netherlands: Kluwer Academic Publishers; 1995:55–65.
23. Mintun MA, Raichle ME, Kilbourn MR, Wooten GF, Welch MJ. A quantitative model for the in vivo assessment of drug binding sites with positron emission tomography. *Ann Neurol.* 1984;15:217–227.
24. Huang SC, Barrio JR, Phelps ME. Neuroreceptor assay with positron emission tomography: equilibrium versus dynamic approaches. *J Cereb Blood Flow Metab.* 1986;6:515–521.
25. Wong DF, Gjedde A, Wagner HN Jr. Quantification of neuroreceptors in the living human brain. I. Irreversible binding of ligands. *J Cereb Blood Flow Metab.* 1986;6:137–146.
26. Pazos A, Probst A, Palacios JM. Serotonin receptors in the human brain-III. Autoradiographic mapping of serotonin-1 receptors. *Neuroscience.* 1987;21:97–122.
27. Hume SP, Ashworth S, Opacka-Juffry J, et al. Evaluation of [*O*-methyl-^{3}H]WAY-100635 as an in vivo radioligand for 5-HT_{1A} receptors in rat brain. *Eur J Pharmacol.* 1994;271:515–523.
28. Mathis CA, Simpson NR, Mahmood K, Kinahan PE, Mintun MA. [^{11}C]WAY 100635: a radioligand for imaging 5-HT_{1A} receptors with positron emission tomography. *Life Sci.* 1994;55:Pl403–Pl407.
29. Pike VW, McCarron JA, Lammerstma AA, et al. First delineation of 5-HT_{1A} receptors in human brain with PET and [^{11}C]WAY-100635. *Eur J Pharmacol.* 1995;283:R1–R3.
30. Lammertsma AA, Bench CJ, Hume SP, et al. Comparison of methods for analysis of clinical [^{11}C]raclopride studies. *J Cereb Blood Flow Metab.* 1996;16:42–52.
31. Ito H, Iida H, Bloomfield PM, et al. Rapid calculation of regional cerebral blood flow and distribution volume using iodine-123-iodoamphetamine and dynamic SPECT. *J Nucl Med.* 1995;36:531–536.
32. Marquardt D. An algorithm for least-squares estimation of nonlinear parameters. *J Soc Indust Appl Math.* 1963;11:431–441.
33. Koeppe RA, Mangner T, Betz AL, et al. Use of [^{11}C]aminocyclohexanecarboxylate for the measurement of amino acid uptake and distribution volume in human brain. *J Cereb Blood Flow Metab.* 1990;10:727–739.
34. Yamaguchi T, Kanno I, Uemura K, et al. Reduction in regional cerebral metabolic rate of oxygen during human aging. *Stroke.* 1986;17:1220–1228.
35. Leenders KL, Perani D, Lammertsma AA, et al. Cerebral blood flow, blood volume and oxygen utilization: normal values and effect of age. *Brain.* 1990;113: 27–47.
36. Khawaja X. Quantitative autoradiographic characterisation of the binding of [^{3}H]WAY-100635, a selective 5-HT_{1A} receptor antagonist. *Brain Res.* 1995;673: 217–225.
37. Carson RE, Channing MA, Blasberg RG, et al. Comparison of bolus and infusion methods for receptor quantitation: application to [^{18}F]cyclofoxy and positron emission tomography. *J Cereb Blood Flow Metab.* 1993;13:24–42.
38. Nyberg S, Farde L, Eriksson L, Halldin C, Eriksson B. 5-HT_2 and D_2 dopamine receptor occupancy in the living human brain: a PET study with risperidone. *Psychopharmacology.* 1993;110:265–272.
39. Vita A, Bressi S, Perani D, et al. High-resolution SPECT study of regional cerebral blood flow in drug-free and drug-naive schizophrenic patients. *Am J Psychiatry.* 1995;152:876–882.
40. Hoyer D, Pazos A, Probst A, Palacios JM. Serotonin receptors in the human brain. I. Characterization and autoradiographic localization of 5-HT_{1A} recognition sites: apparent absence of 5-HT_{1B} recognition sites. *Brain Res.* 1986;376:85–96.
41. Dillon KA, Gross-Isseroff R, Israeli M, Biegon A. Autoradiographic analysis of serotonin 5-HT_{1A} receptor binding in the human brain postmortem: effects of age and alcohol. *Brain Res.* 1991;554:56–64.